JSS Focus Issue on Printable Functional Materials for Electronics and Energy Applications

Electron Field Emission from Water-Based Carbon Nanotube Inks

S. M. Lyth[a,b,*,z] and S. R. P. Silva[c]

[a]*International Institute for Carbon-Neutral Energy Research, Kyushu University, Motooka, Nishi-ku, Fukuoka 819-0395, Japan*
[b]*School of Chemical and Process Engineering, Faculty of Engineering, University of Leeds, Leeds LS2 9JT, United Kingdom*
[c]*Advanced Technology Institute, University of Surrey, Guildford, Surrey GU2 7XH, United Kingdom*

Printable electron field emitters could lead to cheap and scalable large area electron sources. This paper presents work on electron field emission from water-based multiwall carbon nanotube (MWCNT) dispersions, and introduces new results on emission from different substrates. We summarize work in which MWCNTs are deposited onto paper, glass, and plastic substrates, and show that the field emission characteristics can be tailored by controlling the underlying morphology as well as by post-laser irradiation. We also show that engineering the work function of MWCNTs can significantly enhance field emission, and that resonant tunneling effects may be induced by suitable surface functionalization.
 [DOI: 10.1149/2.0051504jss] All rights reserved.

Manuscript submitted November 26, 2014; revised manuscript received January 22, 2015. Published February 11, 2015. *This paper is part of the JSS Focus Issue on Printable Functional Materials for Electronics and Energy Applications.*

Electrons are traditionally confined to the surface of bulk materials by an energy barrier roughly equivalent to the work function (ϕ). They can be thermally excited over this barrier at very high temperatures, in a process known as thermionic emission. However, a more subtle, controllable, and faster means of overcoming the potential barrier at room temperature is to make use of quantum mechanical tunneling. The vacuum energy level in materials is normally flat. However, by applying an electric field one can distort the barrier observed by electrons at the surface, to mimic a triangular potential barrier. Increasing the electric field makes this barrier thinner, and eventually electrons can tunnel from the Fermi level energy states of a metal or semi-conductor into vacuum. This is the basis of electron field emission. The Fowler-Nordheim equation 1 describes the behavior of a generalized field emitting system, where J is the field emission current density, ϕ is the work function, and the constants a and b are 1.54×10^{-6} A(eV)V^{-2} and 6.83×10^{9} $(eV)^{-3/2}$ Vm^{-1}, respectively.[1] The enhancement factor (β) is the factor by which the local electric field at the emitting surface enhances the applied electric field (E), and combines various effects including geometric field enhancement, dielectric field enhancement, and field screening. This enhancement factor depends critically on the surface geometry of an emitter.

$$J = \frac{a\,(\beta E)^2}{\phi} \exp\left(\frac{-b\phi^{\frac{3}{2}}}{\beta E}\right) \qquad [1]$$

From this equation it is clear that the field emitted current can be increased by: i) increasing the applied electric field, ii) decreasing the work function, and iii) increasing the enhancement factor, or by a combination of any of the above factors. By plotting $\ln(J/E^2)$ against 1/E, a "Fowler-Nordheim" plot is obtained, with a gradient of $-b\phi^{3/2}/\beta$, from which β can be calculated. Applications of electron field emission include all fields in which an electron source is required; from flat-screen displays (analogous to flat cathode ray tubes),[2] X-ray sources,[3] field emission microscopy,[4] electron-beam lithography,[5] microwave generation,[6] and space-vehicle thruster charge neutralization.[7]

The covalent bonding in carbon nanotubes (CNTs) makes them ideal field emission materials, with high aspect ratio, strength, stability, electronic conductivity, small diameter and extended length.[8] Most studies focus on aligned CNTs grown by chemical vapor deposition (CVD), and involve various complex processing steps, resulting in impressive but expensive and fragile electron sources.[9,10] Fewer papers have been published on e.g. printed field emission cathodes using CNTs.[11,12] Dispersion of CNTs in a liquid opens the door to a wide variety of deposition techniques such as screen printing, spin-coating, spray coating, drop-casting, stamping, inkjet printing and dip coating.[13] These techniques are cost effective, scalable, with fast processing at room temperature, meaning that CNTs can be deposited or patterned onto a plethora of surfaces including temperature sensitive substrates such as plastic. Electronic devices have been fabricated using screen-printed CNTs for electrochemical sensors,[14] and field emission displays.[15,16] In these cases, the CNTs are generally mixed with an organic binder such as ethyl cellulose. After printing, the substrates are heated to remove the binder. This limits the substrate choice. Dispersing CNTs in water-based inks could be the cheapest and most benign route for printing, by avoiding harmful or expensive organic solvents or binders and minimizing the number of processing steps. As-produced CNTs are hydrophobic and it is therefore difficult to obtain stable dispersions in water without using a dispersant. A common method to form water-based dispersions is by oxidative chemical treatment, resulting in the formation of oxygen containing functional groups on the surface.[17,18] These interact with water molecules via hydrogen bonding. Such water-based CNT inks have been printed using inkjet technology,[19,20] and the dried CNT layer remains stable even after rinsing in water, suggesting that adhesion to the cellulose paper fibers is very strong.[21]

Here we use acid-oxidized multiwall carbon nanotubes (MWCNTs) as a platform to investigate different aspects of electron field emission. Water-based CNT dispersion is applied onto paper, plastic and carbon fibers to demonstrate the versatility of this technique. The effect of underlying substrate morphology and laser irradiation on the field emission properties is investigated. Additionally, the work function is tailored via chemical functionalization in order to increase the emission current, and resonant tunneling effects are discussed. This work reviews our previous publications on the topic as well as presenting new results.

Experimental

MWCNTs (10 nm, Nanocyl) were oxidized in a concentrated H_2SO_4 / H_2NO_3 solution in a procedure outlined elsewhere,[22] resulting in a stable water-based MWCNT dispersion (3.5 mg/ml). The resulting ink was black and opaque, with a consistency similar to that of water. The viscosity is not expected to be significantly different from water at such low concentration (0.0035 wt%).[23,24] This was deposited onto paper, glass (soda lime, Agar Scientific), indium tin oxide coated glass (ITO, Merck), plastic (color laser transparency film, *3 M*),

*Electrochemical Society Active Member.
zE-mail: lyth@i2cner.kyushu-u.ac.jp

and carbon fiber fabric (1071 HCB AvCarb, *Ballard*), via dip coating or spin-coating. Most substrate samples were pre-treated using a microwave plasma system (3 Torr, O_2, Plasma-Preen, Plasmatic Systems Inc.) to render them hydrophilic. Characterization by optical transmission (Cary 5000 UV-Vis-NIR, Varian), scanning electron microscopy (SEM, FEI Quanta 200), and surface roughness (R_A, Sloan Dektak IIA profilometer) was performed. Laser irradiation was carried out using 25 ns pulses from a 248 nm UV excimer laser (Lambda Physik LPX210i, 10^{-4} Torr). Field emission characterization was performed with sphere-plane geometry, using a 5 mm spherical stainless steel anode at $\sim 3 \times 10^{-6}$ Torr.[25] The voltage between anode and earthed sample was incremented in 30 V steps (Keithley model 248). The threshold field (E_{th}) was defined at a current of 1 nA. At least six sites were probed on each sample, and the current was cycled to observe conditioning and hysteresis effects. Some samples were measured in planar configuration to determine current density and electron field emission site densities.

MWCNTs Deposited on Paper

Paper is cheap, robust, widely available, flexible, and has complex cellulose-based microstructure. Utilization of this as a substrate in electronic devices therefore has many advantages. In addition, conventional printing technology goes hand-in-hand with paper substrates. The morphology of a surface plays a crucial role in determining the field emission properties.[28,29] Geometric field enhancement due to micro- and nanoscale protrusions can greatly improve emission. Here, we take advantage of the complex morphology of paper by depositing a thin layer of MWCNTs on the surface, and measuring the field emission characteristics.[26,27] Laser irradiation is used to further modify the microstructure. Paper was obtained from various sources, chosen specifically for the varying but controlled micro-scale structure. This was cut into 1 cm^2 squares, simply dipped into the MWCNT dispersion, carefully removed, and then dried. SEM images show the morphology of samples with the lowest (1.3 μm, Fig. 1a–1c), and the highest surface roughness (9.8 μm, Fig. 1d–1f). The low R_A sample has relatively few, widely-spaced surface features and the high R_A sample has large, closely packed protruding features approximately 25 μm wide. Both samples have uniform MWCNT surface coverage.

Figure 1g shows the current-field characteristics. The different underlying morphology of the paper substrates results in very different field emission characteristics, with a wide range in threshold fields. Little hysteresis is observed, with no conditioning effects. Figure 1h shows Fowler-Nordheim plots. A wide range of gradients is observed, suggesting a wide range in the value of β. E_{th} and β are plotted versus surface roughness in Figure 1i. A clear trend is observed, where the field emission characteristics improve as R_A increases. E_{th} varies widely from 11.6 V/μm at low R_A, to 0.8 V/μm at high R_A. Equivalently, a wide range in β is observed, from 470 at low R_A to 4700 for high R_A substrates (Figure 1j). The very high β is due to a giant multistage geometric enhancement effect arising from the product of the enhancement factors of the paper substrate and the individual MWCNTs.[30] These trends are assumed to be dominated by the varying morphology of the substrates. The high R_A paper substrates have complex morphology with high aspect ratio surface features. This results in high geometric field enhancement, and therefore high β and low E_{th}. Planar field emission measurements reveal a current density at 1.2 V/μm of 27 μA/cm^2.

Subsequently, the best sample was subject to laser irradiation to further modify the surface morphology. Figure 2a–2f shows SEM images of the sample treated with various laser fluences from 0 to 139 mJ/cm^2. In Fig. 2a and 2b no change is observed, because the laser fluence has insufficient energy to modify the surface. In Fig. 2c to 2e, sections of the MWCNT layer peel away from the substrate and protrude from the surface. The degree of surface modification increases as fluence increases. Finally, in Figure 2f a large degree of modification is observed. Some charging is observed where the MWCNTs have been completely removed, exposing the underlying insulating paper. Clusters of individual MWCNTs are observed. It is clear that irradiation with laser light has a profound impact on morphology.

Figure 2g and 2h show the field emission plots. A large range in E_{th} is observed, indicating that irradiation has a significant impact on field emission. As fluence increases, E_{th} decreases and β increases, peaking at a fluence of 111 mJ/cm^2, where E_{th} is 2.1 V/μm and β is 2300 (assuming a work function of 5.1 eV). The error decreases as fluence increases indicating improved uniformity. At 139 mJ/cm^2, a slight deterioration in E_{th} is observed, and β is reduced to 1900.

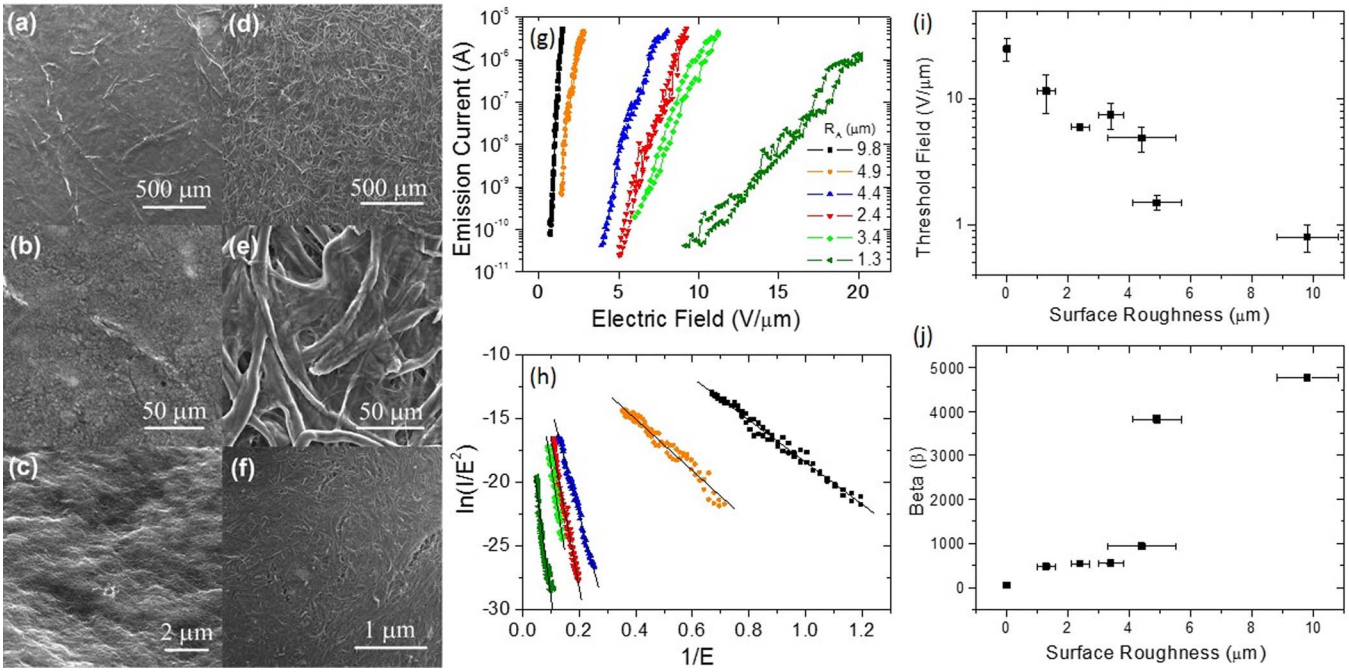

Figure 1. SEM images of (a) to (c); low roughness paper substrate (R_A = 1.3 μm) printed with MWCNT ink, and (d) to (f); high roughness paper (R_A = 4.9 μm) substrate. (g) current-field curves, (h) Fowler-Nordheim plots. Plots of (i) E_{th} and (j) β versus surface roughness.

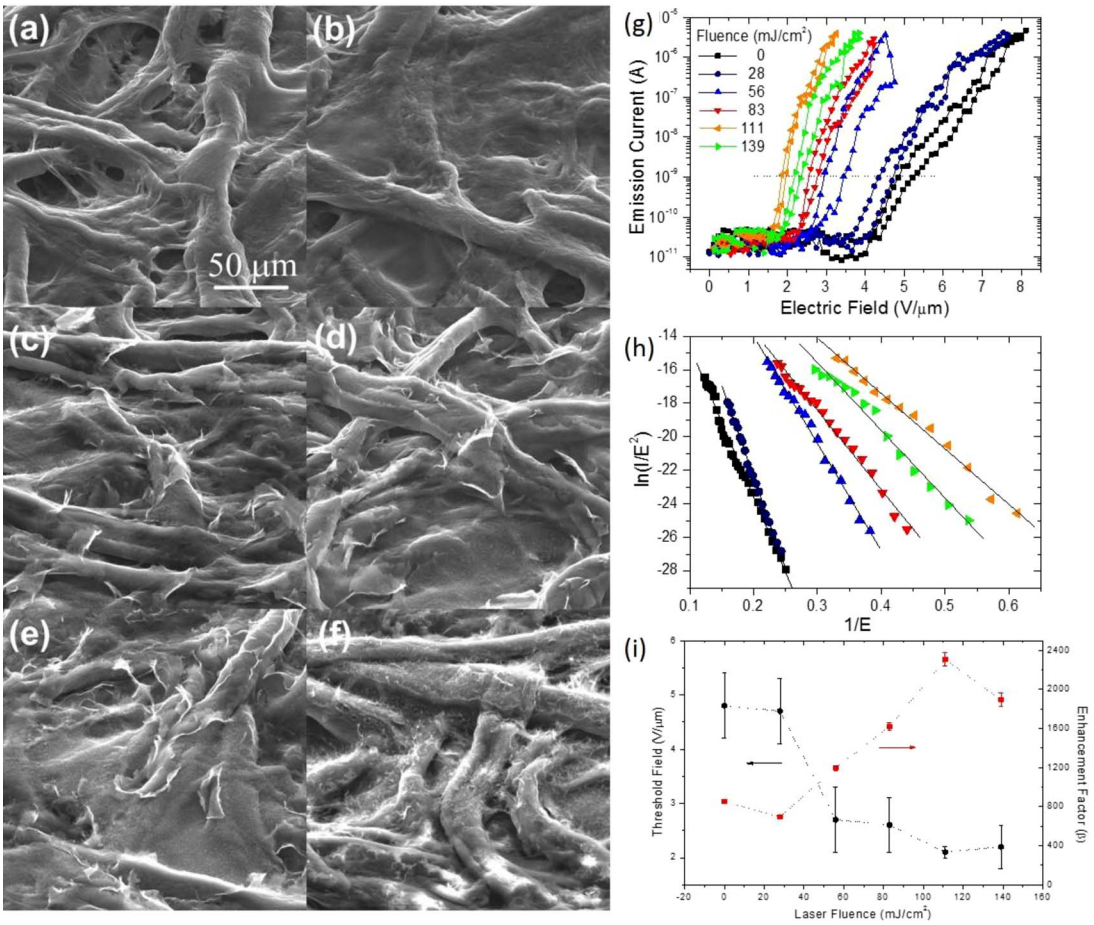

Figure 2. (a-f) SEM images of MWCNTs on paper, irradiated by UV laser light. (g) Current-field curves (h) Fowler-Nordheim plots. (i) E_{th} and β versus laser fluence.

The improvement in field emission with increasing fluence is due to the change in morphology. The protruding MWCNT layers are extremely thin and therefore have high field concentration at their tips, contributing to the high β. At the highest laser fluence, the emission characteristics deteriorate slightly due to extensive surface damage of the sample, leading to lower MWCNT coverage and therefore fewer emitting sites.

Paper-cathode field emission cathodes were incorporated into 3-terminal field emission devices.[31] These devices were fabricated using a unique lamination technique, as a proof of concept that MWCNT-coated paper cathodes can be incorporated into cheap field emission devices via simple large area processing methods. A schematic is shown in Figure 3. Laminate plastic (thickness 60 μm) was sputtered with gold (100 nm) and pierced with 50 μm diameter holes. The cathode was sandwiched between the laminate plastic sheets, and fed through a conventional desktop laminator, bonding the layers together. The MWCNT-coated paper is the cathode; the laminate layer acts as a 60 μm dielectric spacer, and the gold is the gate anode. The total thickness of the device is just 230 μm. Contact to the cathode was made by thin copper wires. In the SEM image (Figure 3b) the gold gate can be seen on the surface and around the edge of the hole.

The field emission properties were first investigated utilizing the gate as an anode, in two-terminal mode (Fig. 3c). Some hysteresis was observed, but the results are remarkably similar to those obtained in sphere-plane geometry. This shows that such techniques can be scaled up to suite large area applications. At 60 V (1 V/μm), the estimated current density is 51 mA/cm^2. Current saturation at high fields may be due to large contact resistance. 3-terminal mode measurements were also performed with a spherical anode. The gate voltage was varied from 0 V to 60 V. Figure 3d shows the field emission current at different gate voltages. From 0 V to 40 V (0.7 V/μm), no current is observed, because the gate voltage is insufficient to extract electrons from the cathode. At 60 V (1 V/μm), a field emission current of 100 nA is detected at an anode voltage of 400 V. These are remarkably good results from such a simple laminated prototype device.

In this section, the field emission characteristics of MWCNTs deposited onto paper substrates were investigated. The field emission was strongly dependent on the underlying morphology, and laser irradiation improved the characteristics significantly by further tuning the surface morphology. MWCNT cathodes on paper substrates were successfully incorporated into a laminated 3-terminal field emission device.

MWCNTs Spin Coated on Glass

Transparent electronics is an important industry with applications in e.g. display technology, sensors, solar cells, touch screens, demisters, and active optical coatings. Transparent CNT films have been extensively researched,[32,33] including in field emission applications.[34,35] Transparent field emitters are likely to have specific applications in the display and lighting markets, where high light transparency is a requirement and transparent emitters could have a beneficial impact on device structure and performance. In this work, glass substrates were first subject to oxygen plasma treatment to render them hydrophilic. MWCNTs were spin coated onto these substrates and dried. This resulted in very smooth films unsuitable for field emission. Therefore the samples were irradiated with UV laser light in order to alter the structure and improve field enhancement, and then the field emission characteristics were investigated.

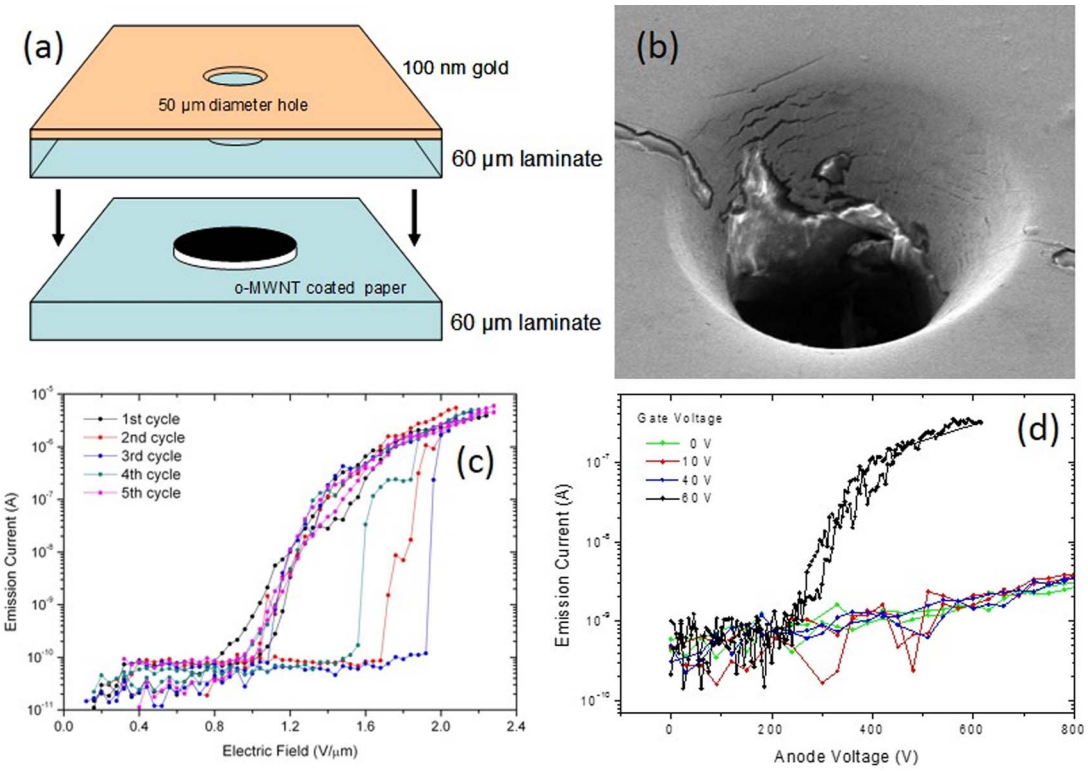

Figure 3. (a) Schematic of a laminated 3-terminal field emission device with a MWCNT cathode on paper. (b) SEM image. (c) 2-terminal current-field characteristics. (d) Field emission current versus applied voltage at varying gate voltages in 3-terminal mode.

Figure 4a–4f shows SEM images after laser treatment. The as-deposited MWCNT layer has high uniformity. After laser irradiation at 172 mJ/cm^2, dark spots (∼1.5 µm diameter) are observed. Higher laser fluence leads to the formation of bright ∼500 nm surface features, possibly formed by melting of the underlying glass. At the highest laser fluence, large patches of MWCNTs are ablated from the surface. Optical transmission measurements at 550 nm show that before laser treatment, the MWCNT layer has 88.7% transmission, falling slightly as fluence increases to 82.7%.

Figure 4g shows the current-field characteristics. Laser treatment results in an improvement in E_{th}. Figure 4h shows Fowler-Nordheim plots. The difference in the gradients suggests that irradiation has

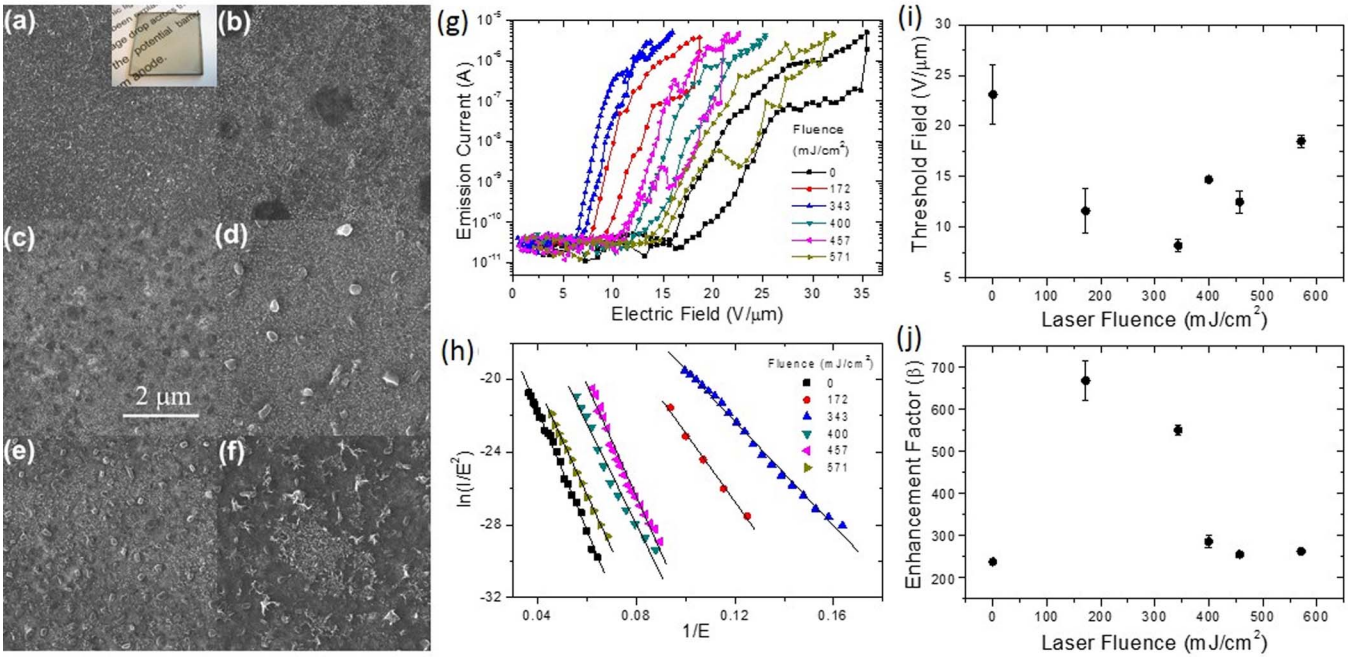

Figure 4. SEM images of MWCNTs spin coated onto glass; (a) before and (b-f) after laser irradiation. Inset: Optical image. (g) Field emission plots. (h) Fowler-Nordheim plots. Laser fluence versus (i) E_{th} and (j) β.

a profound effect on β, as expected from the morphological changes observed in SEM. Before laser irradiation, E_{th} is high (23 ± 2.9 V/μm) and β is low (240 ± 30), due to the extremely smooth underlying substrate (Figures 4i and 4j). The large error indicates that emission uniformity is poor. As the laser fluence increases, E_{th} improves and β increases, peaking at 8 ± 0.6 V/μm and 670 ± 70, respectively, due to the change in morphology. The error in E_{th} is reduced after irradiation, indicating improved uniformity. At even higher fluence, E_{th} degrades to 19 ± 0.6 V/μm and β to 260 ± 30, due to high laser energy density ablating the MWCNTs from the surface.

In this section, it is shown that MWCNTs spin coated on smooth glass substrates have relatively poor field emission characteristics. However, laser irradiation at intermediate fluence modifies the surface morphology of the layer, significantly improving the emission. Higher laser fluences destroy the MWCNT layer, resulting in deterioration of the field emission characteristics.

MWCNTs Spin Coated on ITO Glass

Laser treatment of ITO glass could result in substantially different morphological changes due to the additional effects of the underlying film, potentially leading to further improvements in electron field emission. Therefore, MWCNT layers were spin coated onto ITO glass and irradiated with UV laser pulses of varying fluence. Figure 5 shows SEM images of the irradiated samples, with a photograph (inset). In Figure 5b cracks can be seen in the underlying ITO, because the ITO adsorbs strongly at UV wavelengths. Figure 5c shows slightly wider cracks and clear damage to the MWCNT layer. In Figure 5d a large portion of the MWCNTs have been ablated from the substrate and much larger cracks appear in the ITO layer. In Figure 5e, no MWCNTs are observed as they have been ejected from the surface by the laser pulse. The ITO layer has also been partially destroyed and transported from the surface in large chunks. In Figure 5f, after the highest laser fluence pulse, the ITO layer has melted. Figure 5g shows the current-field plots, from which we can deduce that laser irradiation does indeed result in an improvement in E_{th}. Figure 5h shows Fowler-Nordheim plots, showing that irradiation results in a change of β. The threshold fields and enhancement factors are plotted versus fluence in Figure 5i. Before irradiation, E_{th} is high (18 V/μm) and β is low (170) due to low surface roughness. As fluence increases, E_{th} reaches 6 V/μm and β increases to 810, due to the morphology change in the MWCNT layer. At higher fluence, E_{th} falls to 10 V/μm and β drops to 350, due to ablation of MWCNTs, resulting in fewer emission sites. At the highest fluence, field emission originates from the melted ITO layer, resulting in a better E_{th} and a higher β than the untreated MWCNT layer. The work function of ITO (4.4 eV) is lower than that of carbon, which would also affect the slope of the Fowler-Nordheim plot. The field emission properties measured here are slightly better than those measured on pristine glass substrates, due to the additional morphological changes of the underlying ITO film. Transmission (relative to ITO-coated glass) at the optimum fluence for field emission (186 mJ/cm^2) is 98% (at 550 nm), showing that improvement in the field emission can be achieved while retaining transparency.

In this section MWCNTs spin coated onto ITO-coated glass initially displayed poor field emission characteristics, comparable to those on pristine glass. The field emission was improved by laser irradiation at intermediate fluence, due to a combination of modification of the MWCNT layer morphology, and the morphology of the underlying ITO layer. The field emission characteristics are slightly better

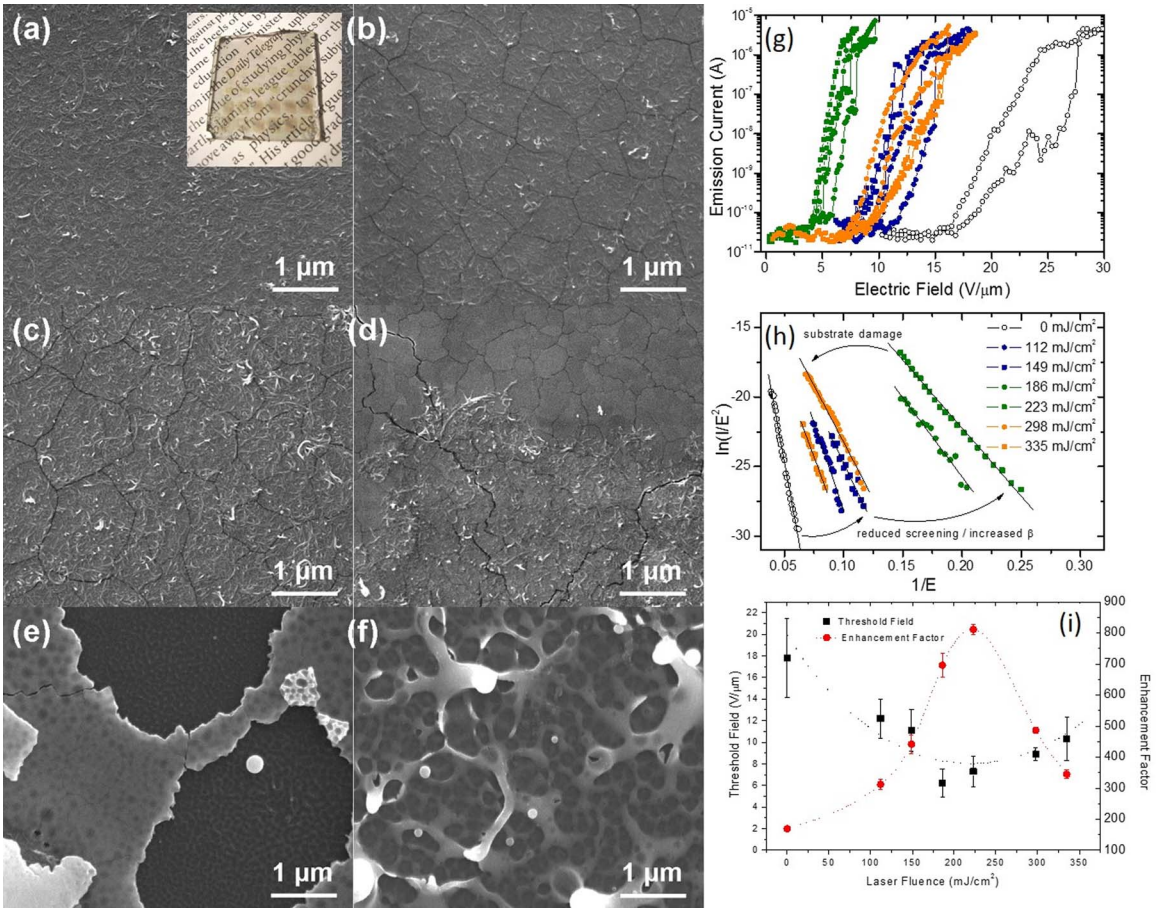

Figure 5. MWCNTs spin coated on ITO glass. SEM images (a) before laser irradiation, and (b-f) after irradiation. Inset: photo of the substrate. (g) Field emission curves. (h) Fowler-Nordheim plots. (i) Laser fluence versus E_{th} and β.

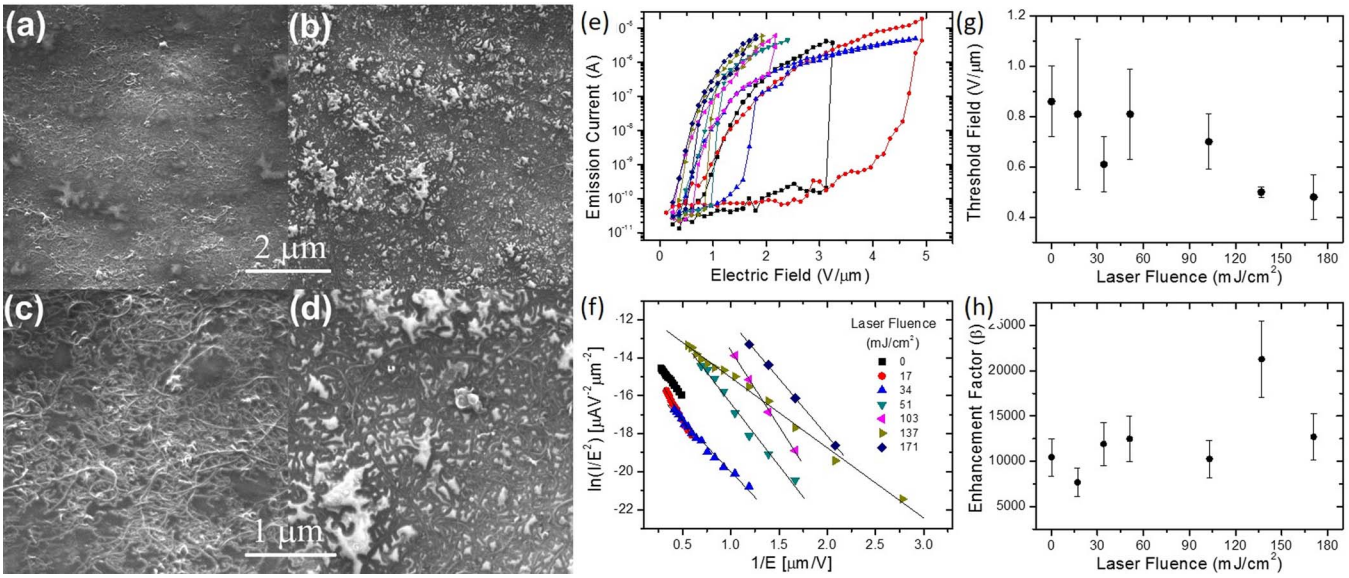

Figure 6. SEM images of MWCNTs spin coated on acetate. (a, c) before and (b, d) after laser irradiation at 17 mJ/cm^2. (e) Current-field plots. (f) Fowler-Nordheim plots. (g) E_{th} versus laser fluence and (h) β versus laser fluence.

than those of MWCNTs on pristine glass, suggesting that the underlying ITO has some influence. At high laser fluence, the MWCNT layer is destroyed and the emission characteristics deteriorate.

MWCNTs Spin Coated on Acetate

Depositing MWCNTs from water-based dispersion onto plastic substrates allows for cheap, flexible transparent electrodes. The melting point of plastic is lower than glass and therefore greater impact on morphology is also expected under laser irradiation. Samples were prepared by spin coating MWCNTs onto O_2-plasma treated acetate sheets, followed by laser irradiation. Figure 6a and 6c shows images before irradiation, and Figure 6b and 6d after irradiation with laser fluence of 17 mJ/cm^2. In the untreated sample, the MWCNT layer can clearly be observed. However, the coverage is not complete and the substrate can be observed in places. After laser treatment, the substrate appears as bright spots, possibly indicating that the substrate is carbonized by the laser and becomes more conductive. At higher fluence it was impossible to obtain SEM images, due to charging effects. Figure 6e shows current-field characteristics and Figure 6f shows Fowler-Nordheim plots. The samples have very low threshold fields even before laser irradiation, although the hysteresis values are extremely large. Laser irradiation results in improved E_{th} and reduced hysteresis. Figure 6g and 6h show E_{th} and β as a function of fluence. Before irradiation, E_{th} is already only 0.9 V/μm with a large β of 10400. As fluence increases, E_{th} gradually decreases to 0.5 V/μm at 171 mJ/cm^2. Optical transmission at 550 nm (with respect to air) was 80.5% before laser treatment, and 70.0% at 171 mJ/cm^2.

Current density measurements were carried out in a planar field emission cell, with an anode gap of 970 μm and an emitting area of 0.585 cm^2 (Fig. 7a). The field emission curves are similar to those in Figure 6 and E_{th} is of the order expected. Figures 7b–7e show photographs of the cell with a phosphor anode. Figure 7b shows the cell at zero bias. At 3 V/μm, a small emission spot is observed (c). At 4 V/μm, the single emission spot burned out, and large areas of the sample started to emit (d). After reducing the voltage back down to 3 V/μm, the sample still emitted uniformly (e). After this conditioning process, the current density was 100 μA/cm^2 at 1 V/μm.

In this section MWCNTs spin coated onto transparent acetate substrates were found to display surprisingly low threshold fields but with very large hysteresis. Laser irradiation improved the threshold fields

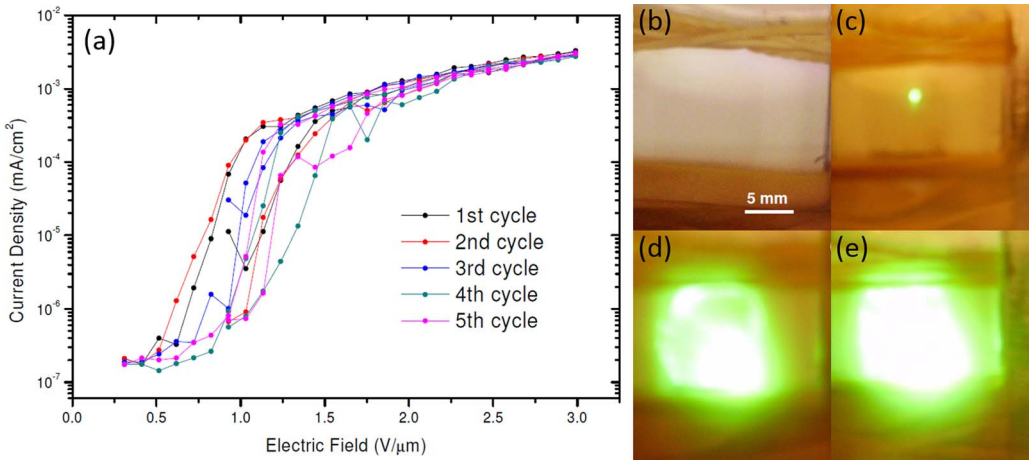

Figure 7. Planar field emission measurements of MWCNTs on acetate. (a) Current density versus applied electric field. Photographs of a planar field emission cell with a phosphor anode at (b) zero bias, (c) 3 V/μm, (d) 4 V/μm and (e) back at 3 V/μm.

and reduced hysteresis effects. In planar configuration, uniform field emission was obtained after an initial conditioning step.

Work Function Engineering of MWCNTs

In the previous sections, β was tailored via substrate morphology or laser irradiation in order to improve the field emission from MWCNT cathodes, by texturing the surface. However, the Fowler-Nordheim equation suggests that lowering the work function can also increase the field emission current. If this could be achieved, it would provide a simple method for improving field emission cathodes without the need to physically modify the surface morphology. However in practice, tailoring the work function of CNTs is not straight forward as it is a fundamental property of a material. Several methods to overcome this have been reported, for example by using low work function coatings,[37,38,39] or intercalation of low work function compounds.[40,41] Chemical methods of changing the work function of CNTs are much more promising, being scalable, performed in aqueous media, and at ambient temperature. The work function of MWCNTs is particularly sensitive to acid oxidative treatments, in which oxygen containing moieties (e.g. carboxyl groups) form on the surface.[42] These disrupt the π-conjugation and introduce inward-pointing surface dipole moments, leading to a higher work function (from 4.3 eV to 5.1 eV).[43] However, secondary chemical reactions performed on these groups can be used to reduce the work function, because the surface dipole is sensitive to the nature of the associated cation. For example, alkali cation exchange with lithium can be used to reduce the work function from 5.1 eV to 4.6 eV.[44] Here, we engineer the work function of oxidized MWCNTs using a simple, scalable, room temperature chemical reaction, namely lithium functionalization via alkali metal cation exchange.[36] Water-based dispersions of these modified MWCNTs can be deposited onto substrates as in the previous sections.

Lithium cation exchange (Figure 8e) was achieved by dispersing 4×10^{-4} moles of LiOH per mg of acid oxidized MWCNTs in 2 ml of HPLC grade deionized water. Solutions were thoroughly mixed in an ultrasonic bath for 30 minutes prior to filtration and then washed with pure water until the filtrate was pH neutral, ensuring the removal of excess hydroxide. Carbon fiber fabric was subjected to a 10-second microwave O_2 plasma treatment, and then dip coated into the MWCNT inks. The samples were then removed and baked at 100°C for 20 minutes to remove residual water. Figure 8a shows an SEM image of the pristine carbon fiber, (b) after oxygen plasma treatment, and (c) after being coated with MWCNTs, which form a uniform layer covering the whole carbon fiber surface.

Field emission characteristics were investigated in sphere-plane geometry with a typical electrode gap of 3 mm. Electrical connection was made via back contacts of conductive carbon adhesive tabs. Figure 8f shows the current-field curves, in which the different samples clearly have very different field emission characteristics, and that lithium treated MWCNTs have much improved properties compared with pristine MWCNTs. Carbon fiber fabric has an E_{th} of 0.42 ± 0.03 V/μm. After oxygen plasma treatment, E_{th} rises to 0.58 ± 0.15 V/μm, attributed to the increase in work function due to the introduction of oxygen-containing functional groups. Coating the carbon fiber with MWCNTs results in a decrease in E_{th} to 0.42 ± 0.09 V/μm, attributed to the increased geometric field enhancement of the MWCNT layer. Coating with lithium functionalized MWCNTs results in a further decrease of E_{th} to 0.25 ± 0.02 V/μm, attributed to the lowering of the work function from 5.1 eV to 4.6 eV. The extremely low error suggests very good uniformity across the substrate. Fowler-Nordheim plots are presented in Figure 8g, and β is similar for all the samples. These results show that work function engineering is a viable and low cost method to tailor field emission properties.

In this section, work function engineering was used to improve the field emission properties of MWCNTs, as opposed to modifying the enhancement factor via surface morphology (as in the previous sections). Reducing the work function from 5.1 to 4.6 eV corresponded to a decrease in threshold field from 0.42 to 0.25 V/μm. Engineering

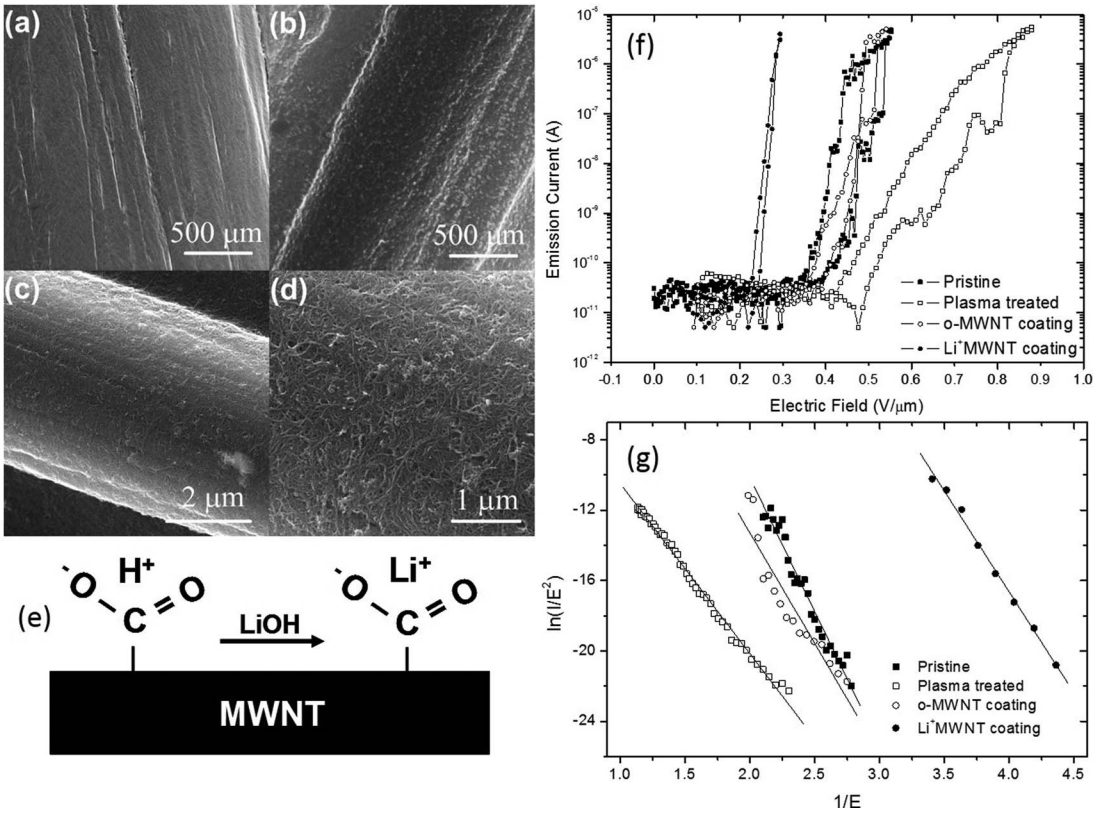

Figure 8. SEM images of (a) carbon fiber, (b) oxygen plasma-treated carbon fiber (c) MWCNT coated carbon fiber, (d) lithium-functionalized MWCNT coated carbon fiber. (f) Current-voltage characteristics. (g) Fowler-Nordheim plots.

the work function of water-based MWCNT inks in this manner is a simple and cheap way to improve the field emission properties of carbon-based materials.

Resonant Tunneling

Close analysis of field emission currents from acid oxidized MWCNTs on carbon fiber substrates reveals unexpected staircase-like increases in current density, also reflected in the Fowler-Nordheim plots. These characteristics are analyzed in more detail.[45] Figure 9a shows emission current with increasing field, and (b) shows Fowler-Nordheim plots. Repeatable staircase-like features are observed in the emission current. The current rises in steps of approximately one order of magnitude and the width of the steps is ~0.047 V/μm. This behavior is highlighted in a derivative plot of the data (Figure 9e). The Fowler-Nordheim graph shows a similar staircase-like form. Figure 9c shows the emission current in a decreasing field, and Figure 9d shows the corresponding Fowler-Nordheim plots. These also display staircase behavior, but distinctly different from Figure 9a and 9b, with only two larger steps of unequal width.

This behavior is attributed to resonant tunneling through surface functional groups and/or the adsorbed water molecules associated with these functional groups, giving rise to a quantum well structure at the MWCNT surface. The multiple steps observed in the current-field data represent multiple electronic energy levels confined in potential wells at the surface. Non-linearity in the field emission current occurs due to resonance when the electronic sub-levels in the quantum well are aligned with the Fermi level of the MWCNT, and negative differential resistance occurs when the sub-levels are unaligned. The difference between the increasing and decreasing field emission currents may be due to slow decharging due to trapped states in the quantum well. Figure 9f shows a schematic potential diagram, in which the functional groups or adsorbate is assumed to take the form of a square potential well. Electrons are more likely to tunnel from metal to vacuum through the energy levels of the adsorbate, due to a reduction in the effective thickness of the barrier.

These staircase-like characteristics have not been commonly observed due to the high field resolution necessary to resolve the individual current steps (each being only 0.047 V/μm wide). This was achievable here due to the very low threshold fields of these cathodes. However, similar effects have been observed under different conditions.[46] Field emission is strongly influenced by adsorbates. In 1967, Duke and Alferieff showed that resonant tunneling through the energy levels of atoms and molecules adsorbed on metal surfaces plays a major role in field emission.[47] In field emission microscopy the emitted current can increase if an atom or molecule is adsorbed onto the local probe area due to resonance tunneling enhancement.[5] More recently, resonant tunneling through localized surface states in chemisorbed molecules has been used to explain the lobed patterns observed in field emission microscopy from CNT caps.[48] Resonant tunneling through surface states is utilized in scanning tunneling microscopy.[49,50,51] Resonant tunneling has also been predicted for field emission from multilayer $Si\text{-}SiO_2\text{-}Si\text{-}SiO_2$ cathodes.[52]

In this section, non-linearity in the field emission currents from acid-oxidized MWCNT cathodes was explained in terms of resonant tunneling through surface functional groups and/or water molecules adsorbed on the surface. These effects could only be observed due to the high data resolution in these experiments and the very low threshold fields achieved. These experiments show that chemical processing of carbon-based field emission cathodes cannot only be used to tailor the work function, but also to induce resonant tunneling effects into the emission current, with potential applications in field emission microscopy or scanning tunneling microscopy.

Summary

In this work, we explored the field emission characteristics of water-based multiwall carbon nanotube dispersions, prepared by acid functionalization. These were deposited onto various different substrates by spin coating, or dip coating. When coated onto paper substrates, a clear relation between the surface roughness of the MWCNT support and the emission characteristics emerged. As surface roughness increased, the threshold field decreased, due to modification of the enhancement factor and decreased field screening. The lowest threshold field achieved using this technique was 0.8 V/μm. Laser irradiation was performed on the MWCNT paper cathodes in an

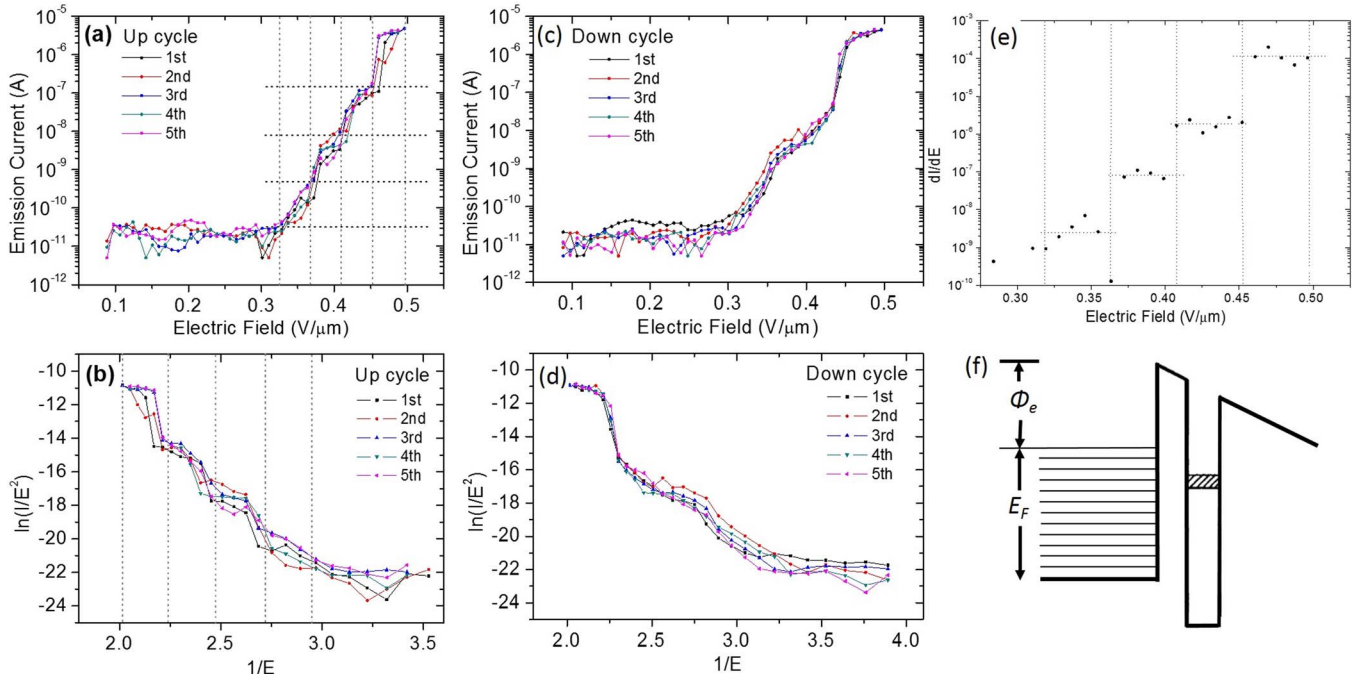

Figure 9. (a) Current-field curves for acid-oxidized MWCNTs deposited on carbon fiber substrates (with increasing field) and (b) the same data plotted in Fowler-Nordheim coordinates. (c) Current field curves (with decreasing field) (d) plotted in Fowler-Nordheim coordinates. (e) Derivative plot of the field emission characteristics. (f) Schematic representation of the band structure.

attempt to improve the field emission characteristics by modification of the surface morphology. A significant improvement in threshold field was observed with increasing laser fluence, followed by deterioration at very high fluence. This trend is attributed to clear modification of the morphology of the MWCNT layer by the incident laser light, increasing field enhancement. At high fluence the MWCNT layer is ablated from the paper, reducing the field emitted current. A prototype field emission device was fabricated by laminating MWCNT-coated paper cathodes in gold-sputtered acetate sheets, pierced with holes of 50 μm diameter. This was operated in both 2-terminal and 3-terminal configuration, and a current density of 51 mA/cm^2 was achieved. This device is extremely simple to make, and is a proof-of-concept that large area field emission devices could be produced by roll-to-roll manufacturing techniques.

The fabrication of transparent field emission cathodes was also investigated. MWCNT inks were spin-coated onto glass substrates, which were then subjected to laser irradiation in order to alter the morphology and increase field enhancement. As-spun MWCNT layers had extremely poor field emission characteristics due to the extremely smooth nature of the underlying substrate. The threshold field decreases with increasing laser fluence, due to modification of the morphology of the MWCNT layer, which improves field enhancement. At high laser fluence, the field emission characteristics deteriorate due to ablation of the MWCNTs from the surface of the glass. A similar study was performed on ITO-coated glass substrates, and it was found that the ITO layer is additionally modified by incident laser energy, leading to an extra level of surface modification, and further improved threshold fields. The use of acetate as a flexible transparent MWCNT support was investigated, and very low threshold fields were recorded, down to around 0.5 V/μm after laser irradiation. However, the hysteresis was very large. Uniform emission across the whole area of the cathode was achieved in 2-terminal configuration with a phosphor anode after an initial conditioning cycle, with a current density of 0.1 mA/cm^2 at 1 V/μm.

Lithium cation exchange was utilized in aqueous solution to modify the work function of MWCNT inks, which were then deposited onto carbon fiber substrates by dip coating. Lithium functionalization reduces the work function of acid oxidized MWCNTs from 5.1 to 4.6 eV, resulting in a significant improvement in threshold field from 0.42 to 0.25 V/μm. This simple solution-based chemical method of changing the work function could be applied on a large scale. Finally, stepped increases in the field emission current were observed in acid oxidized MWCNT inks deposited onto carbon fiber substrates. These were revealed only because of the very low threshold fields and the resulting high data resolution. This behavior was attributed to resonant tunneling through the surface functional groups and/or adsorbed water molecules, and shows that quantum effects can be measured and manipulated in large area field emission cathodes, with possible applications in field emission microscopy.

Conclusions

In conclusion, the above studies all utilize MWCNT inks deposited onto a variety of surfaces (paper, glass, ITO, plastic, carbon fiber) as large area field emission cathodes. The importance of the substrate is highlighted, with morphology and surface roughness affecting the field emission directly by influencing the enhancement factor via geometric field enhancement. Simply put, rougher substrates result in better field emission properties. Laser irradiation also enhances the field emission properties by direct modification of the MWCNT layer morphology, again increasing the enhancement factor via geometric field enhancement. The only other method to increase field emission current is to vary the work function. This is not usually straightforward, but here lithium cation exchange in aqueous solution is utilized to this end, resulting in a direct improvement in field emission properties. These results show that large-scale manufacturing techniques such as aqueous chemical functionalization, water-based ink processing (including printing), large area laser irradiation, and lamination could be utilized in field emission technologies.

Acknowledgments

Stephen M. Lyth is currently supported by World Premier International Research Center Initiative (WPI), MEXT, Japan, and also gratefully acknowledges funding from the International Research Center for Hydrogen Energy, Kyushu University.

References

1. R. H. Fowler and L. Nordheim, *Proceedings of the Royal Society of London. Series A*, 173–181 (1928).
2. A. A. Talin, K. A. Dean, and J. E. Jaskie, *Solid-State Electronics*, **45**(6), 963 (2001).
3. Z. Liu, G. Yang, Y. Z. Lee, D. Bordelon, J. Lu, and O. Zhou, *Applied Physics Letters*, **89** (10), 103111 (2006).
4. G. Ehrlich, *Advances in Catalysis*, **14**, 255 (1963).
5. X. Chen, S. H. Zaidi, S. R. J. Brueck, and D. J. Devine, *Journal of Vacuum Science & Technology B*, **14**(5), 3339 (1996).
6. J. H. Han, T. Y. Lee, D. Y. Kim, J. B. Yoo, C. Y. Park, J. J. Choi, and J. M. Kim, *Diamond and related materials*, **13**(4), 987 (2004).
7. S. Marcuccio, A. Genovese, and M. Andrenucci, *Journal of Propulsion and Power*, **14**(5), 774 (1998).
8. C. H. Poa, S. R. P. Silva, P. C. P. Watts, W. K. Hsu, H. W. Kroto, and D. R. M. Walton, *Appl. Phys. Lett.*, **80**, 3189 (2002).
9. M. T. Cole, K. B. K. Teo, O. Groening, L. Gangloff, P. Legagneux, and W. I. Milne, *Sci. Rep.*, **4**, 4840 (2014).
10. M. Chhowalla, K. B. K. Teo, C. Ducati, N. L. Rupesinghe, G. A. J. Amaratunga, A. C. Ferrari, and W. I. Milne, *Journal of Applied Physics*, **90**(10), 5308 (2001).
11. J. Li, W. Lei, X. Zhang, X. Zhou, Q. Wang, Y. Zhang, and B. Wang, *Applied surface science*, **220**(1), 96 (2003).
12. F. Zeng, C. C. Zhu, W. Liu, and X. Liu, *Microelectronics journal*, **37**(6), 495 (2006).
13. A. S. Alshammari, M. Shkunov, and S. R. P. Silva, *Phys. status solidi - Rapid Res. Lett.*, **8**, 150 (2014).
14. J. Wang and M. Musameh, *Analyst* **129**, 1 (2004).
15. W. B. Choi, D. S. Chung, J. H. Kang, H. Y. Kim, Y. W. Jin, I. T. Han, Y. H. Lee, J. E. Jung, N. S. Lee, G. S. Park, and J. M. Kim, *Appl. Phys. Lett.* **75**, 3129 (1999).
16. J. Li, W. Li, X. Zhang, X. Zhou, Q. Wang, Y. Zhang, and B. Wang, *Appl. Surf. Sci.* **220**, 96 (2003).
17. M. S. P. Shaffer, X. Fan, and A. H. Windle, *Carbon* **36**, 1603 (1998).
18. R. A. Hatton, A. J. Miller, and S. R. P. Silva, *J. Mater. Chem.*, **18**, 1183 (2008).
19. Z. Fan, T. Wei, G. Luo, and F. Wei, *J. Mats. Sci.*, **40**, 2461 (2005).
20. K. Kordas, T. Mustonen, G. Toth, H. Jantunen, M. Lajunen, C. Soldano, S. Talapatra, S. Kar, R. Vajita, and P. M. Ajayan, *Small* **2**, 1021 (2006).
21. A. J. Miller, R. A. Hatton, and S. R. P. Silva, *Appl. Phys. Lett.*, **89**, 123115 (2006).
22. N. P. Blanchard, R. A. Hatton, and S. R. P. Silva, *Chemical physics letters*, **434**(1), 92 (2007).
23. P. Garg, J. L. Alvarado, C. Marsh, T. A. Carlson, D. A. Kessler, and K. Annamalai, *Int. J. Heat Mass Transf.*, **52**, 5090 (2009).
24. J. C. Grunlan, L. Liu, and O. Regev, *J. Colloid Interface Sci.*, **317**, 346 (2008).
25. R. C. Smith and S. R. P. Silva, *Appl. Phys. Lett.*, **94**, 133104 (2009).
26. S. M. Lyth and S. R. P. Silva, *Applied physics letters*, **90**(17), 173124 (2007).
27. S. M. Lyth, S. J. Henley, and S. R. P. Silva, *Journal of Vacuum Science & Technology B*, **27**(3), 1068 (2009).
28. L. Nilsson, O. Groening, C. Emmenegger, O. Kuettel, E. Schaller, L. Schlapbach, H. Kind, J. M. Bonard, and K. Kern, *Appl. Phys. Lett.* **76**, 2071 (2000).
29. R.C. Smith, R.D. Forrest, J.D. Carey, W.K. Hsu, and S.R.P. Silva, *Appl. Phys. Lett.* **87**, 013111 (2005).
30. J. Y. Huang, K. Kempa, S. H. Jo, S. Chen, and Z. F. Ren, *Appl. Phys. Lett.* **87**, 053110 (2005).
31. S. M. Lyth, L. D. Filip, D. C. Cox, and S. R. P. Silva, *IEEE 20th International Vacuum Nanoelectronics Conference (IVNC)*, 241–242 (2007).
32. Z. C. Wu, Z. H. Chen, X. Du, J. M. Logan, J. Sippel, M. Nikolou, K. Kamaras, J. R. Reynolds, D. B. Tanner, A. F. Hebard, and A. G. Rinzler, *Science* **305**, 1273 (2004).
33. G. D. M. R. Dabera, K. D. G. I. Jayawardena, M. R. R. Prabhath, I. Yahya, Y. Y. Tan, N. A. Nismy, H. Shiozawa, M. Sauer, G. Ruiz-Soria, P. Ayala, V. Stolojan, A. A. D. T. Adikaari, P. D. Jarowski, T. Pichler, and S. R. P. Silva, *ACS Nano*, **7**, 556 (2013).
34. A. N. Banerjee and K. K. Chattopadhyay, *Appl. Surf. Sci.* **225**, 243, (2004).
35. Y. H. Li, Y. M. Zhao, M. Roe, D. Furniss, Y. Q. Zhu, S. R. P. Silva, J. Q. Wei, D. H. Wu, and C. H. P. Poa, *Small* **2**, 1026 (2006).
36. S. M. Lyth, R. A. Hatton, and S. R. P. Silva, *Applied physics letters*, **90**(1), 013120 (2007).
37. S. Dimitrijevic, J. C. Withers, V. P. Mammana, O. R. Monteiro, J. W. Ager III, and I. G. Brown, *Appl. Phys Lett*, **75**, 2680 (1999).
38. A. Wadhawan and R. E. Stallcup II, J. M. Perez, *Appl. Phys. Lett.* **78**, 108 (2001).
39. F. Jin, Y. Liu, and C. M. Day, *Appl. Phys. Lett.* **88**, 163116 (2006).
40. S. Suzuki, C. Bower, Y. Watanabe, and O. Zhou, *Appl. Phys. Lett.* **76**, 4007 (2000).
41. B. Ha and C. J. Lee, *Appl. Phys. Lett*, **90**, 023108 (2007).

42. P. C. P. Watts, N. Mureau, Z. Tang, Y. Miyajima, J. D. Carey, and S. R. P. Silva, *Nanotechnology*, **18**, 175701 (2007).
43. H. Ago, T. Kugler, F. Cacialli, W. R. Salaneck, M. S. P. Shaffer, A. H. Windle, and R. H. Friend, *J. Phys. Chem. B.* **103**, 8116 (1999).
44. N. P. Blanchard, R. A. Hatton, and S. R. P. Silva, *Chem. Phys. Lett.* **434**, 92 (2007).
45. S. M. Lyth and S. R. P. Silva, *Applied Physics Letters*, **94**(12), 123102 (2009).
46. S. Johnson, U. Zülicke, and A. Markwitz, *Journal of applied physics*, **101**(12), 123712 (2007).
47. C. B. Duke and M. E. Alfereiff, *J. Chem Phys.* **46**, 923 (1967).
48. K. A. Dean and B. R. Chalamala, *J. Appl. Phys.* **85**, 3832 (1999).
49. C. J. Chen, *Phys. Rev. Lett.* **65**, 448 (1990).
50. I. Martin, A. V. Balatsky, and J. Zaanen, *Phys. Rev. Lett.* **88**, 097003 (2002).
51. K. Bobrov, A. J. Mayne, and G. Dujardin, *Nature*, **413**, 616 (2001).
52. Y. V. Kryuchenko and V. G. Litovchenko, *Journal of Vacuum Science & Technology B*, **14**(3), 1934 (1996).